QUT

Queensland University of Technology
Brisbane Australia

Alloying Gold with Copper Makes for a Highly Selective Visible Light Photocatalyst for the Reduction of Nitroaromatics to Anilines

Qi Xiao,[†] Sarina Sarina,[†] Eric R. Waclawik,[†] Jianfeng Jia,[‡] Jin Chang,[†,Δ] James D. Riches,[§] Haishun Wu,[‡] Zhanfeng Zheng,[||] and Huaiyong Zhu*,[†]

[†]School of Chemistry, Physics and Mechanical Engineering, Science and Engineering Faculty, Queensland University of Technology, Brisbane, QLD 4001, Australia

[‡]School of Chemical and Material Science, Shanxi Normal University, Linfen 041004, China

[Δ]Institute of Advanced Materials (IAM), National Jiangsu Synergistic Innovation Center for Advanced Materials (SICAM), Nanjing Tech University, Nanjing 211816, China

[§]Institute for Future Environments & School of Earth, Environmental and Biological Sciences, Queensland University of Technology, Brisbane, QLD 4001, Australia

[||] State Key Laboratory of Coal Conversion, Institute of Coal Chemistry, Taiyuan 030001, China

ABSTRACT: Finely controlling product selectivity is an essential issue in organic chemical production. In the synthesis of functionalized anilines via reduction of the corresponding nitroarenes, the challenge is to selectively reduce only the nitro group in the presence of other reducible functional groups in nitroarene molecules at a high reaction rate. Normally, the nitroarene is reduced stepwise through a series of intermediates, which remain as by-products, increasing the aniline synthesis cost. Here we report that alloying small amounts of copper into gold nanoparticles can alter the reaction pathway of the catalytic reduction under visible light irradiation and at ambient temperatures, so that nitroaromatics transform directly to anilines in a highly selective manner. The reasons for the high efficiency of the photocatalytic reduction under these comparatively benign conditions as well as the light excited reaction mechanisms were discussed. This photocatalytic process avoids by-products, exhibits high reaction rate, excellent substituent tolerance, and can be used for synthesis of many useful functionalized anilines under environmentally benign conditions. The switching of reaction pathway by simply tailoring the bimetallic alloy NPs of the photocatalysts is effective for engineering product chemoselectivity.

KEYWORDS: *Au-Cu alloy, photocatalysis, reduction, reaction pathways, visible light*

■ INTRODUCTION

Nitroaromatic compounds are among the most important industrial chemicals in use today.[1] For example, approximately 95% of nitroarenes are consumed in the production of anilines, which are important precursors to rubber chemicals, pesticides, dyes, explosives, and pharmaceuticals.[2] An essential issue with this reduction process is achieving high product selectivity.[3-6] Many useful anilines contain reducible functional groups. It is a challenge to reduce the nitro group only, at high reaction rate, while maintaining any other reducible groups in the reactants unchanged.[3,5,6] The selective reduction process has been extensively studied using a variety of heterogeneous catalytic systems.[3-6] In those reported catalytic systems, the reduction proceeds via the well-known pathways first proposed by Haber in 1898 (Figure 1).[7] The nitro group of the reactant is stepwise reduced to a corresponding aniline through nitroso and hydroxylamine intermediates.[8-11] Condensation of the reactive intermediates yields coupling derivatives such as azobenzene and azoxybenzene.[10,11] But conversions from azoxy- to azo-compound and from azo-compound

to aniline are slow steps.[11] These steps involve the cleavage of the last O-N bond and addition of H to the azo group, respectively, high reaction temperature and high pressures of hydrogen are used to accelerate the process, even though excellent catalysts were discovered. These conditions can reduce other functional groups in the reactants.
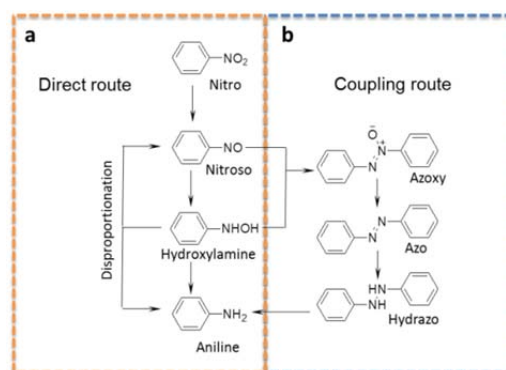

Figure 1. Reaction pathways for the reduction of aromatic nitro compounds to the corresponding anilines proposed by Haber. (a) direct route. (b) coupling route.

Previously we reported that Au nanoparticles (NPs) supported on catalytically inert zirconium oxide (ZrO_2) can exhibit high catalytic activity for the selective transformation of nitroaromatics to their corresponding azo-compounds in an isopropanol solution under visible light irradiation at 40°C.[12] The supported Au NPs strongly absorb visible light due to the localized surface plasmon resonance (LSPR) effect and efficiently channel the light energy to the reactant, inducing reaction at moderate reaction conditions.[13-15] The photocatalytic reduction using supported Au NPs also proceeds via Haber's pathways as intermediate azoxy-compound and trace over-reduced product aniline were observed. When this photocatalytic system is used to produce functional anilines from nitroarenes, high selectivity towards the aniline product is difficult to achieve.

To address the issue of high selectivity toward aniline, discovery of catalytic systems that proceed by a different reaction mechanism from Haber's long established pathway could prove useful. If there is a viable, new route to producing aniline as sole product, solving the high selectivity issue is a fundamentally important consideration. In the present study, we find one such photocatalytic system. Au-copper (Cu) alloy NPs with a small Cu fraction were prepared, and it was found that reduction catalyzed by these Au-Cu alloy NP photocatalysts, under visible light irradiation, at ambient temperature, do not follow Haber's reaction pathways, but rather yield the corresponding anilines directly as the sole product. The photocatalytic process can be used to selectively reduce the nitro group in the presence of other reducible groups in the reactant nitroarenes to yield functionalized anilines, which has remained a challenge in controlling this reduction process.

■ RESULTS AND DISSCUSSION

A series of catalysts of Au-Cu alloy NPs supported on ZrO_2 were prepared as the photocatalyst (for experimental details, see Experimental Section). ZrO_2 was chosen as the support because it is a catalytically inert material in the present study and can be used to achieve a homogeneous distribution of metal NPs on the surface.[12] The total metal amount of the catalyst was maintained at 3 wt%, which was an optimal metal loading based on our previous work,[12] and the Au:Cu ratio was varied to obtain several alloy catalysts (labelled $Au_{3-x}Cu_x@ZrO_2$, e.g. $Au_{2.6}Cu_{0.4}@ZrO_2$ catalyst containing 2.6 wt% Au and 0.4 wt% Cu). The $Au_{2.6}Cu_{0.4}@ZrO_2$ catalyst exhibited superior photocatalytic activity, and the aniline yield under irradiation was approximately 3.6 fold that of the control reaction in the dark (Figure 2a). The photocatalytic performance of the catalysts with varied Au:Cu ratios for the reduction was also investigated and summarized in Figure 2a. Importantly, the catalysts exhibited unique selectivity to aniline, whereas Au NP catalyzed reactions have produced mainly azobenzene. The selectivity behavior changed as a function of

Au/Cu composition, when the Cu content was 0.4~0.6 wt% (and the corresponding Au content was 2.6~2.4 wt%), the product selectivity was solely aniline. (Figure 2b). The product selectivity of the nitrobenzene reduction catalyzed by $Au_{2.6}Cu_{0.4}@ZrO_2$ is compared with that catalyzed by $Au_{3.0}@ZrO_2$ catalyst under the same conditions as shown in Figures 3a and 3b. The control experiments in the dark show similar trend in the product selectivity, but lower conversion rate under the identical reaction conditions (Figures 3c and 3d).
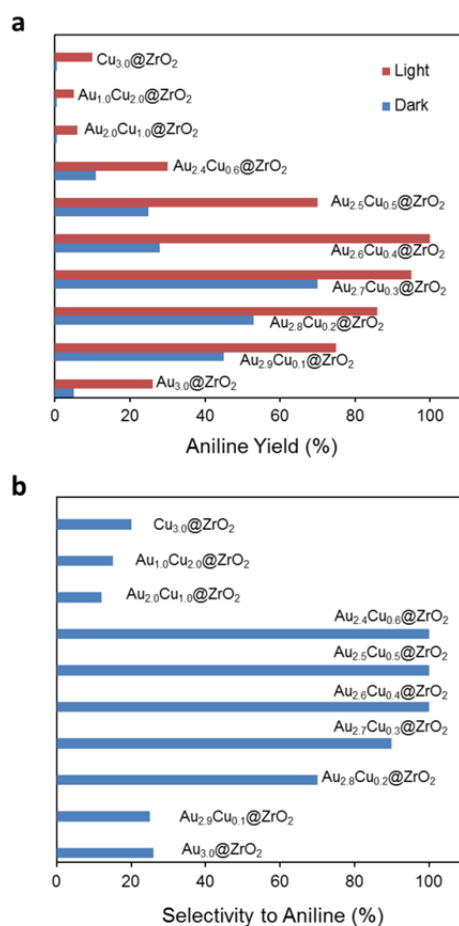

Figure 2. Photocatalytic performance for the reduction of nitrobenzene. (a) Au-Cu alloy NPs @ZrO_2 catalysts with varied composition. (b) The dependence of the product selectivity to aniline on the Au-Cu alloy NPs @ZrO_2 catalysts with varied Au/Cu composition under visible light irradiation.

It is evident that the direct reduction of nitrobenzene to aniline using the Au-Cu alloy NP catalyst is distinctly different from reductive coupling of nitrobenzene catalyzed by a Au NP catalyst. When $Au_{2.6}Cu_{0.4}@ZrO_2$ catalyst was used (Figure 3a), the selectivity to aniline approached 100% from the initial reaction stage and remained at 100% until the reaction completed. In contrast, when a pure Au NP photocatalyst was used there was no aniline product in the early reaction stage (Figure 3b). The nitrobenzene conversion reached 100% within 3 h, which was faster than occurred with Au-Cu alloy NPs, however the main product was azobenzene. Azoxybenzene was generated in the initial stage of the reaction (0.5 h). As the
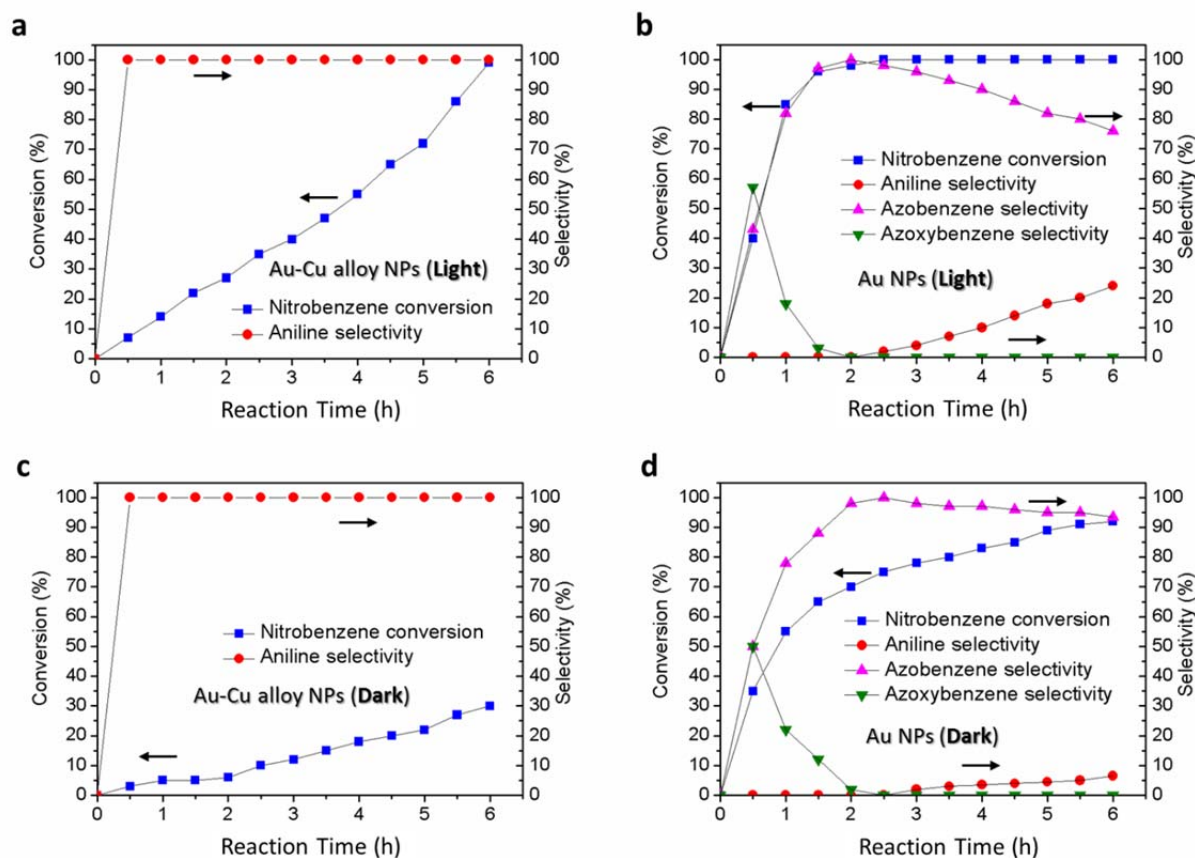
Figure 3. (a)Time-conversion plot for nitrobenzene reduction using $Au_{2.6}Cu_{0.4}@ZrO_2$ catalyst under visible light irradiation. (b) Time-conversion plot for nitrobenzene reduction using $Au_{3.0}@ZrO_2$ catalyst under visible light irradiation. (c)Time-conversion plot for nitrobenzene reduction using $Au_{2.6}Cu_{0.4}@ZrO_2$ catalyst in the dark. (b) Time-conversion plot for nitrobenzene reduction using $Au_{3.0}@ZrO_2$ catalyst in the dark. Reaction conditions: the reactions were conducted in an argon atmosphere at 40 °C using 2 mL of isopropyl alcohol mixed with 0.025 mmol KOH, 0.1 mmol of nitrobenzene and 50 mg of catalyst. The irradiation intensity was 0.5 W/cm^2, and the reaction time was 6 h. For the dark reactions, all the reaction conditions were kept identical with the photocatalytic reactions except keeping the reaction tubes out of light.

reaction proceeded, the selectivity towards azoxybenzene dropped substantially over the course of the reaction, while the selectivity towards azobenzene significantly increased (0.5~2 h). The azobenzene selectivity reached 100% within 2 h, and then declined as aniline emerged as the further reduced product. The aniline selectivity was also much lower at the end of the six hour reaction, compared with that using Au-Cu alloy NPs as the photocatalyst. The complex sequence of reactions and intermediates formed in this process with the pure Au NP catalyst indicate that the photocatalytic coupling follows the pathways proposed by Haber.[7,10,11] In contrast, the reduction catalyzed by Au-Cu alloy NPs does not.

The photocatalytic coupling of nitrobenzene on the pure Au NP surface does not consume the reducing agent except in the initial stage,[12] while the direct reduction of nitrobenzene to aniline should. Isopropyl alcohol was the reducing agent in the photocatalytic reduction, which provided hydrogen and was oxidized to acetone. The content of acetone in the reaction system catalyzed by the Au-Cu alloy NPs increased gradually as the reaction proceeded (Figure 4), in

proportion with the aniline yield. Both reactants exist in liquid phase and have adequate access to the catalyst dispersed in the liquid. This is part of the reason why the reaction can proceed at ambient pressure, which leads to significant saving in the cost of the reactor. The catalyst can be readily recycled after reactions without significantly losing activity (for details, see Figure S1 in SI).
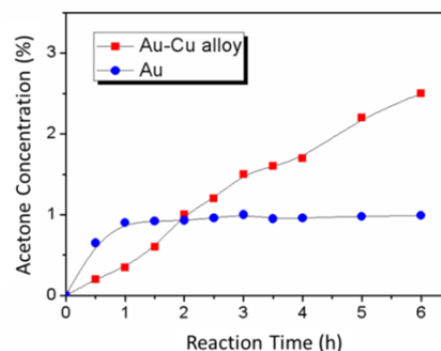

Figure 4. The time-conversion plot for acetone formation during the reduction of nitrobenzene under visible light

irradiation using $Au_{2.6}Cu_{0.4}@ZrO_2$ and $Au_{3.0}@ZrO_2$ catalysts respectively.

Figures 5a and 5b show typical transmission electron microscopy (TEM) images of the $Au_{2.6}Cu_{0.4}@ZrO_2$ catalyst. The mean size of the alloy NPs was 5 nm. The lattice fringes of Au-Cu alloy NPs can be observed from the high resolution TEM (HR-TEM) image in Figure 5b. The lattice fringe spacing of 0.22 nm corresponds to the interplanar distance of Au-Cu alloy (111) planes.[16] The energy dispersive X-ray spectroscopy (EDS) line scan analysis of a Au−Cu alloy NP indicates that Au and Cu were uniformly distributed in the alloy NP (inset in Figure 5a). This was also apparent in the EDS mapping and X-ray photoelectron spectroscopy (XPS) analysis provided in Figure S2 and S3 in SI, the Au content was much higher than the Cu content. The characterization results confirmed the formation of $Au_{2.6}Cu_{0.4}$ alloy NPs.
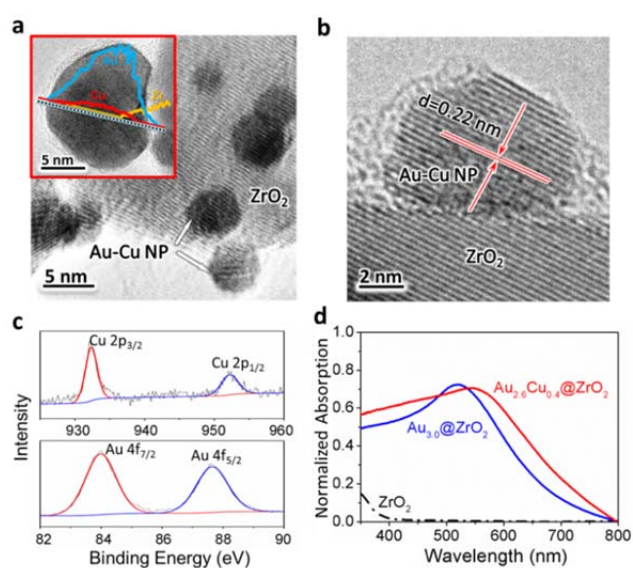

Figure 5. Characterization of the photocatalyst. (a) Typical TEM image of $Au_{2.6}Cu_{0.4}@ZrO_2$; inset: line profile analysis providing information about the elemental composition and Au/Cu distribution of a NP. (b) HR-TEM images of the typical $Au_{2.6}Cu_{0.4}$ alloy NP. (c) XPS profile of Cu and Au species in the $Au_{2.6}Cu_{0.4}$ alloy NPs. (d) UV/Vis spectra of $Au_{2.6}Cu_{0.4}@ZrO_2$ and monometallic $Au_{3.0}@ZrO_2$ catalyst.

A challenge for Cu-based NP catalysts is that O_2 in air can oxidize surface Cu atoms of alloy NPs, which will result in the rapid loss of activity during reactions exposed to air.[17] It is known that the Cu oxidation rate depends on alloy NP composition, and that increasing amounts of Au can improve catalyst stability.[18] In bulk Au-Cu alloys Au can protect Cu from oxidation by limiting Cu_2O surface island growth.[19] Thus, we anticipate that Au-Cu alloy NPs with a low Cu content are stable in air. The pattern of XPS in Figure 4c confirmed this. The binding energies of Cu 2p1/2 at around 952.0 eV and Cu 2p3/2 at 932.5 eV can be mainly attributed to the Cu^0 state.[20,21] However, due to the small loading amount of Cu, and low signal

intensity the analysis of the Cu Auger lines for an assignment of Cu^0 and Cu^{1+} was not possible.[22] Sugano *et al* suggested that, in the AuCu alloy NP photocatalyst, the partial oxidized surface Cu atoms could be successfully reduced by plasmon-activated Au atoms and maintain the AuCu alloying effect.[23] Thus even if there is very small amount of Cu oxide existing on the surface, it could be reduced to metallic state under irradiation.[23,24] The binding energies of Au are identical to the bulk of gold metal.[25]

The light absorption property is an important characteristic for a photocatalyst. The monometallic Au NP catalyst exhibits a distinctive light absorption band at 525 nm due to the LSPR effect (Figure 5d). In comparison, a red-shift of the LSPR band was observed for the Au-Cu alloy NPs, which is also evidence of alloying (Figure 5d and Figure S4, SI).[26] Characterizations of the photocatalysts, however, could not provide a direct explanation for the dramatic change in product selectivity. To gain insight into the reaction pathway of the process with the alloy photocatalyst, reductions of the possible intermediates (nitrosobenzene, phenylhydroxylamine and their mixture) were conducted using $Au_{2.6}Cu_{0.4}@ZrO_2$ and monometallic $Au_{3.0}@ZrO_2$ catalyst, respectively, with the other experimental conditions maintained identical to those for the nitrobenzene reduction (Table 1).

Table 1. Reaction pathway study of catalytic performance using $Au_{2.6}Cu_{0.4}@ZrO_2$ and monometallic $Au_{3.0}@ZrO_2$ catalysts for various intermediates as substrates.
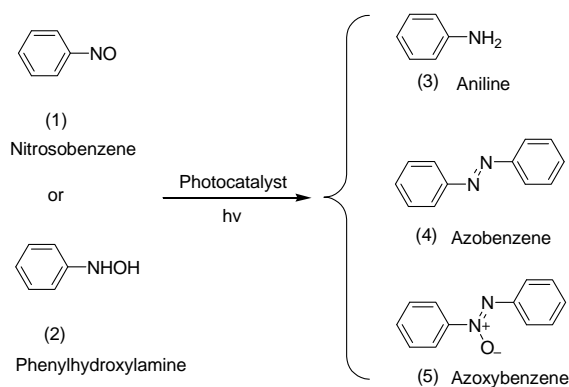
Entry	Substrate	Catalyst	Conv.(%)	Sel.(%)		
				3	4	5
1[a]	1	Au-Cu	100	5	3	85
2[a]	1	Au	100	4	4	83
3[b]	2	Au-Cu	100	19	6	75
4[b]	2	Au	100	15	85	0
5[b]	1+2	Au-Cu	100	4	3	93
6[b]	1+2	Au	100	8	92	0
7[c]	4	Au-Cu	70	100	0	0
8[c]	4	Au	55	10[d]	-	0

Reaction conditions: the reactions were conducted in an argon atmosphere at 40°C using 2 mL of isopropyl alcohol mixed with 0.025 mmol KOH, 0.1 mmol substrate (for entries 5 and 6: 0.05 mmol of substrate 1 and 0.05 mmol of substrate 2 were used), and 50 mg of catalyst. The irradiation intensity was 0.5

As shown in entries 1 and 2 (Table 1), if nitrosobenzene was the reactant, then azoxybenzene was the main product no matter which catalyst was used, and the product selectivities were very similar. However, when phenylhydroxylamine was the reactant (Table 1, entries 3 and 4), a striking difference in the product selectivity was observed: the main product with the alloy NP catalyst was azoxybenzene while only a small fraction of azobenzene was detected (Table 1, entry 3). The main product with monometallic Au NP catalyst was azobenzene, and no azoxybenzene was observed (Table 1, entry 4). The reaction proceeded rapidly and completed within 1 h, indicating that phenylhydroxylamine was highly reactive. The small amounts (19% and 15%) of aniline in the product could have formed via a disproportionation pathway simultaneously with the coupling route as proposed in Figure 1, which is based on literature.[10]

Further experiments using the mixture of nitrosobenzene and phenylhydroxylamine as reactants gave similar results (Table 1, entries 5 and 6). The reaction between nitrosobenzene and phenylhydroxylamine could occur spontaneously (without catalyst) and rapidly, yielding mainly azoxybenzene, as soon as they were mixed. Thus, we can exclude the formation of intermediates such as nitrosobenzene and phenylhydroxylamine in the reduction using Au$_{2.6}$Cu$_{0.4}$@ZrO$_2$ catalyst, because if they formed in the reaction, either of them would result in the coupling products. Comparison of the results of entry 2 with those of entries 4 and 6 indicates that phenylhydroxylamine was the key intermediate to afford the main product azobenzene in the reaction catalyzed by monometallic Au NPs (Table 1). Moreover, the Au-Cu alloy NPs can also catalyze the reduction of azobenzene to the sole product aniline with 100% selectivity within 16 h under visible light irradiation, whereas pure Au NPs are slow to yield the aniline product even after prolonged reaction time (Table 1, entries 7 and 8). This suggests that formation of aniline on Au-Cu alloy surface is highly favored, while pure Au NPs exhibit a much weaker ability to catalyze the hydrogenation of azobenzene to aniline, thus the Au NP surface has selectivity towards azobenzene in the reduction process.

We propose a reaction pathway that would explain this difference as shown in Figure 6. Analysis confirmed that the monometallic Au NPs catalyzed the reaction via Haber's coupling route. By this pathway, the final product aniline was obtained mainly after the coupling step (azoxy→ azo→ hydrazo→ aniline). In the reaction system of the present study, H-Au species form on the surface of metal NPs as isopropanol provides hydrogen while being oxidized to acetone.[12] The H-Au species can react with nitrobenzene to yield nitrosobenzene. According to Haber's mechanism, nitrosobenzene is a reactive intermediate, it will transform to phenylhydroxylamine rapidly.[10,11] This is the reason why nitrosobenzene was not detected during the reaction. High concentration of phenylhydroxylamine favors formation of azobenezne on Au NPs (Table 1, entries 4 and 6). Blaser proposed that Haber's coupling route is favored under basic conditions.[10] This is certainly true in the case of the monometallic Au catalyst. When Au-Cu alloy NPs were used as photocatalysts, nitrobenzene transformed directly to a sole product aniline, we did not detect any by-product such as azobenzene or other intermediate during the reaction. The detailed mechanistic understanding of this phenomenon is still unclear, which may need further future work to explore in detail. Interestingly, even in basic conditions (KOH was added into the reaction system) the reduction catalyzed by Au-Cu alloy NPs followed the direct reduction route.
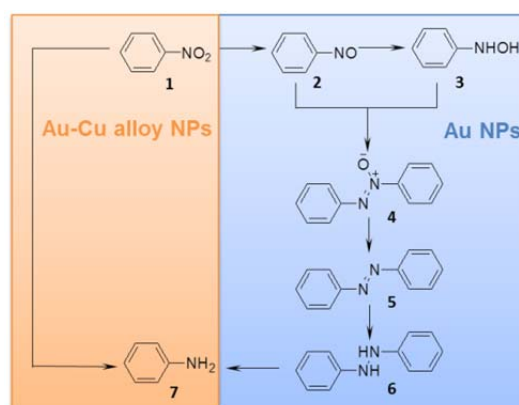

Figure 6. The proposed reaction pathway for the reduction of nitrobenzene in the present study.
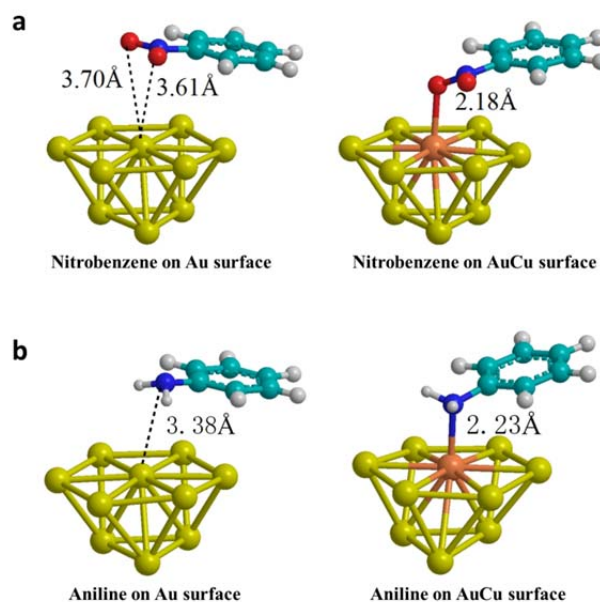

Figure 7. The DFT simulated nitrobenzene (a) and aniline (b) on Au and Au-Cu alloy surface. The nitrobenzene molecule has much stronger interaction with Au-Cu alloy surface compared with that on pure Au surface (a). When aniline molecule is adsorbed on Au-Cu alloy surface, the N atom in the aniline molecule is attracted by the Cu atom and the length of N–Cu bond is 2.23 Å. However, when

aniline molecule is close to the surface of Au surface, the N atom was repelled as shown in the figure (b). The interaction of the N atom of the nitrobenzene or aniline molecules with Cu atom in Au-Cu alloy NPs is much stronger than that with Au atoms on NP surface.
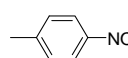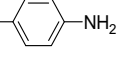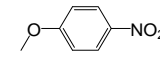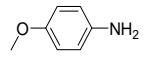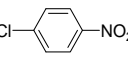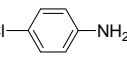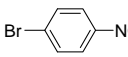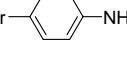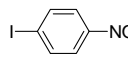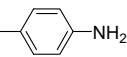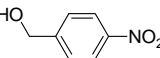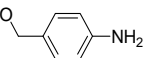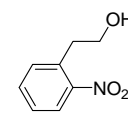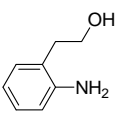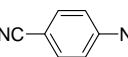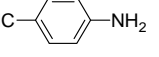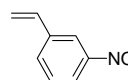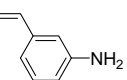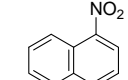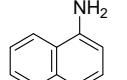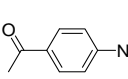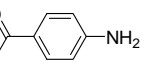
To further understand the reason why aniline was the sole product of the reaction catalyzed by Au-Cu alloy NPs, we performed a density functional theory (DFT) simulation study on the adsorption of the reactant nitrobenzene and the product aniline on the surfaces of Au and Au-Cu clusters, respectively (Figure 7 and Table S1, SI). The DFT simulation results indicate that both the reactant nitrobenzene and the product aniline adsorb more strongly to the Au-Cu alloy surface than to the pure Au surface. The interaction of the N atom of the nitrobenzene or aniline molecules with a Cu atom in the Au-Cu alloy NPs is much stronger than that with Au atoms on the NP surface. This immobilizes the reactant molecules adsorbed at Cu atom sites of the alloy NP surface. The mobility of the reactant molecules is a prerequisite for the coupling reaction, so in contrast to Au-Cu alloy, the reactant molecules (intermediate molecules with N atom) on a pure Au surface are labile and can move for coupling. The immobilized reactant molecules on the Cu atoms will be directly reduced to aniline. The product aniline is also much more stable on a Au-Cu alloy surface than on a pure Au surface. The simulation results confirm that formation of aniline on the Au-Cu alloy surface is favored thermodynamically, compared with that on Au NP surface. Moreover, considering the difference in surface electronic properties between the alloy NPs and pure Au NPs, the electronegativity of Au is 2.54, being much stronger than that of Cu (1.90).[27] There are electron-rich sites of Au and slightly positively charged sites of Cu at the surface of alloy NPs. The interaction between aniline and positively charged sites is stronger than that between aniline and pure Au NP surface. Hence, thermodynamically the formation of aniline on the alloy surface is more favorable than that on the pure Au surface; and thus alloying Au with Cu in the present study always enhances the product selectivity to aniline.

The isopropyl alcohol was the reducing agent and firstly oxidized to acetone yielding H–Au NP[12,28] or H–Cu NP species.[20] Given the large Au content in the alloy NPs, the H–Au NP species are considered to play the major role in reacting with the oxygen atoms of N–O bonds in the nitrobenzene to induce the reduction on the surface of the alloy NPs.

The general applicability of the Au-Cu alloy NP-photocatalyzed reduction of nitroaromatics was studied. Table 2 shows the results for the reduction of nitroaromatics to anilines with $Au_{2.6}Cu_{0.4}@ZrO_2$ catalyst under visible light irradiation and in the dark. Visible light irradiation promoted each reaction; the yields of the light irradiated reactions were much higher than that of the reactions in the dark for all reactions. The products were the corresponding anilines, no coupling product such as azo- or azoxy-compounds were detected. For the reduction of halogen-containing nitroaromatics, dehalogenation could sometimes be

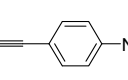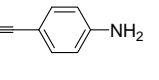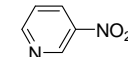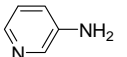inevitable. In our case, the dehalogenation was suppressed and quantitative conversion of these substrates can be realized (Table 2, entries 3-5).

Table 2. Photocatalytic reduction of substituted nitroaromatics using $Au_{2.6}Cu_{0.4}@ZrO_2$ catalyst.

Entry	Reactant	Product		Yield (%)
1	—⬡—NO₂	—⬡—NH₂	Light	95
			Dark	36
2	O—⬡—NO₂	O—⬡—NH₂	Light	89
			Dark	40
3	Cl—⬡—NO₂	Cl—⬡—NH₂	Light	63
			Dark	24
4	Br—⬡—NO₂	Br—⬡—NH₂	Light	90
			Dark	20
5	I—⬡—NO₂	I—⬡—NH₂	Light	40
			Dark	0
6	HO—⬡—NO₂	HO—⬡—NH₂	Light	45
			Dark	8
7	OH / ⬡—NO₂	OH / ⬡—NH₂	Light	100
			Dark	23
8	NC—⬡—NO₂	NC—⬡—NH₂	Light	100
			Dark	34
9	⬡—NO₂ (vinyl)	⬡—NH₂ (vinyl)	Light	95
			Dark	29
10	naphthalene-NO₂	naphthalene-NH₂	Light	85
			Dark	36
11ᵃ	O=⬡—NO₂	O=⬡—NH₂	Light	65
			Dark	0
12ᵇ	≡—⬡—NO₂	≡—⬡—NH₂	Light	64
			Dark	0
13ᶜ	⬡(N)—NO₂	⬡(N)—NH₂	Light	45
			Dark	0

The reactions were conducted in an argon atmosphere at 40°C using 2 mL of isopropyl alcohol mixed with 0.025 mmol KOH, 0.1 mmol of reactant, and 50 mg of $Au_{2.6}Cu_{0.4}@ZrO_2$ catalyst. The irradiation intensity was 0.5 W/cm², and the reaction time was 6 h. ᵃ100 mg of $Au_{2.6}Cu_{0.4}@ZrO_2$ catalyst and reaction temperature 60°C. ᵇ0.05 mmol of reactant, 2 mL of mixed solvent (isopropyl alcohol:tetrahydrofuran = 1:1), 100 mg of $Au_{2.6}Cu_{0.4}@ZrO_2$ catalyst, reaction temperature 60°C, and the reaction time was 48 h. ᶜReaction temperature 60°C, and the reaction time was 16 h. The product selectivity to anilines was 100%. The yield was calculated from the product formed and the reactant converted, as measured by GC.

The most-challenging substrates are those that bear other easily reducible moieties. The reduction of these substrates allows production of important products: functionalized anilines. The $Au_{2.6}Cu_{0.4}@ZrO_2$ catalyst was observed to not only be able to reduce nitro groups

in the presence of alkenes (Table 2, entry 9), but could also reduce them in the presence of alkynes without detectable concurrent reduction of the unsaturated unit (Table 2, entry 12). Nitrile, keto substituents or heteroarene functioned groups were unaffected as well. Paracetamol (N-acetyl-p-aminophenol) is a major ingredient in numerous analgesic, cold and flu remedies.[29] Typically, it is produced by reducing 4-nitrophenol to 4-aminophenol, then acetylated with acetic anhydride.[29] The reduction of 4-nitrophenol is the key step, and H_2 or $NaBH_4$ are the widely used reductants. The reaction can be easily monitored by UV-vis spectroscopy.[30-32] In the present study, we found that 4-nitrophenol can be selectively reduced to 4-aminophenol using Au-Cu alloy NP catalyst under irradiation (Figure S5, SI).

Evidently, the Au-Cu alloy NP catalyst is an efficient photocatalyst for selective reduction of nitroaromatics directly to functionalized anilines using visible light under mild reaction conditions compared to those reported elegant works.[3-6] To achieve higher catalytic rate, we simply increased the reaction temperature slightly from 40 °C to 60 °C for several substrates under typical reaction conditions (Table S2, SI). The reactions can achieve 100% conversion within 45 min, and still maintain the high chemoselectivity to reduce the nitro groups. This is due to the continuum of metal electron energy levels in the metal NP photocatalysts, which provides the capacity to couple the stimuli of irradiation and heat to drive reactions.[33,34] This is an apparent merit compared with traditional heterogeneous catalysts and semiconductor photocatalysts.

In the photocatalytic process the light drives the reduction and reductive coupling by exciting metal electrons, the light-excited electrons (so-called hot electrons) provide the activation energy required for the cleavage of the N–O bond. This conclusion is supported by the fact that the catalytic activity of $Au_{2.6}Cu_{0.4}@ZrO_2$ photocatalyst for the reduction of nitrobenzene to aniline significantly depends on the irradiation intensity (Figure 8a). When the irradiation intensity was raised, the aniline yields increased, and at the higher the intensity the contribution of irradiation to the overall reaction rate is greater. A higher irradiation intensity will excite more hot electrons populate above the Fermi level of the metal NPs, which can facilitate the reactions, as reported for AuNPs.[33-39] Moreover, when the irradiation intensity was maintained constant, we found that the reaction rate is higher at the wavelength absorbed more strongly by the catalyst for a number of reductions as shown in action spectrum of the reactions.[20,35-37] Such an action spectrum is shown in Figure 8b. In the action spectrum, the apparent quantum yield (AQY) of the reduction is closely related to the irradiation wavelength. The action spectrum of the reduction of nitrobenzene to aniline using $Au_{2.6}Cu_{0.4}@ZrO_2$ photocatalyst shows that the AQY for aniline yield matches well the light absorption of the alloy NP catalyst. The highest yield is achieved under the irradiation with the wavelength, where the alloy NPs have the most intense absorption due to the LSPR effect.

The hot electrons activate the reaction by two ways: Firstly, the hot electrons transfer to the molecular orbital of the reactant molecules adsorbed on the metal NP surface,[40] which is associated to the chemical bond (N-O bonds) to be cleaved. There is an energetic requirement for hot electron transfer: the hot electrons have energy above a threshold, which depends on the energy level of the molecular orbital associated with the N-O bonds.[41] The hot electrons with sufficient energy can transfer into the reactant molecules and weaken the N-O bonds, resulting in the reaction. Secondly, although low intensity illumination on plasmonic metal NP, most likely does not play a role in inducing chemistry, particularly in continuous-flow,[42] the hot electrons can dissipate their energy via electron-phonon interaction to heat the lattice of the NPs,[41] especially when the hot electrons do not have sufficient energy for the direct transfer to the adsorbed reactant molecules.[41]

If the light energy absorbed by the hot electrons dissipates entirely as heat in the NPs, the AQY depends on the light absorption at all wavelengths. The higher AQY is observed at the wavelength more intensively absorbed by the catalyst. Nonetheless, if the energy threshold for the hot electron transfer is low, such dependence can also be observed. The reduction of nitrobenzene is likely to have a low energy threshold (Figure 8b).

Figure 8c displays a different action spectrum for the reaction using 4-nitrobenzyl alcohol as substrate: the reaction AQY value is greater at shorter wavelengths (such as 400 nm and 470 nm) although the most intensive light absorption of the catalyst appears at 560 nm. It is also noted that the AQY values at wavelengths of 590 nm and 620 nm are approximately 1/6 of the values at 400 nm and 470 nm, while the light absorption at the long wavelengths are about 20% less than those at the short wavelengths. Hence, the photothermal effect cannot have induced such large difference in the AQY values. Actually, the AQY values at wavelengths of 590 nm and 620 nm provide an approximate measure for photothermal effect. Evidently for this reaction, cleaving of the N-O bonds is predominantly driven by hot electron transfer.

We noted that the yield of 4-nitrobenzyl alcohol reduction is much lower than that of nitrobenzene reduction (Table 2). This means that it is more difficult to cleave the N-O bonds in 4-nitrobenzyl alcohol with the hot electrons excited by the LSPR light absorption, compared with that in nitrobenzene. The alcohol group substituted on the aromatic ring raises the energy level of the LUMO associated with the N-O bonds (Figure 8d). The hot electrons generated in the metal by shorter wavelength irradiation have enough energy (Figure 8d, left), to effectively activate 4-nitrobenzyl alcohol molecules for reaction. It is therefore rational that the N-O bond-cleaving reaction is predominately driven by hot electron transfer with a high energy threshold in this case.
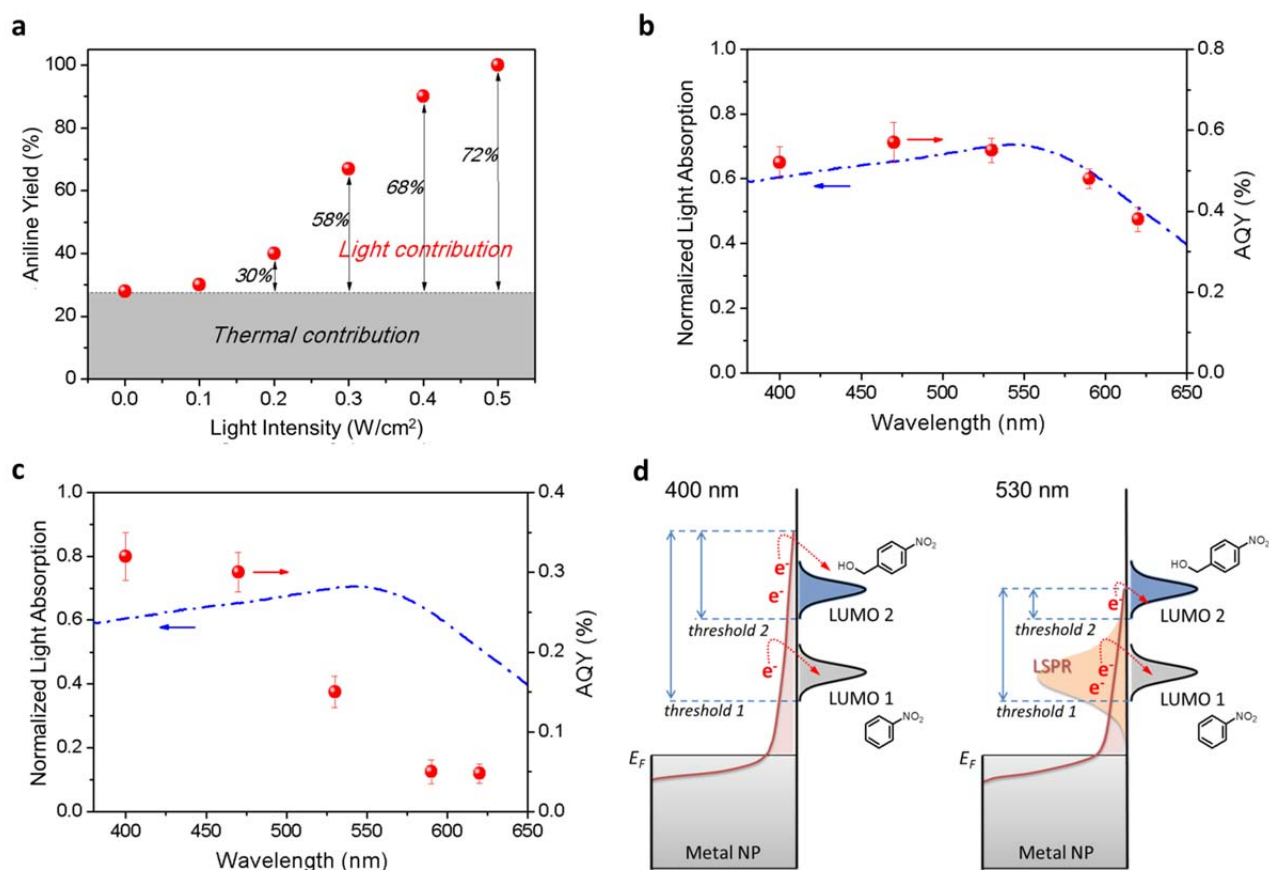
Figure 8. The impact of light intensity and wavelength. (a) The dependence of the catalytic activity of Au$_{2.6}$Cu$_{0.4}$@ZrO$_2$ photocatalyst for the reduction of nitrobenzene to aniline on the intensity of the light irradiation. The percentages inside of the figure show the contribution of the light irradiation effect. (b) Action spectrum for the photocatalytic reduction of nitrobenzene using Au$_{2.6}$Cu$_{0.4}$@ZrO$_2$ catalyst. (c) Action spectrum for the photocatalytic reduction of 4-nitrobenzyl alcohol using Au$_{2.6}$Cu$_{0.4}$@ZrO$_2$ catalyst. (d) Hot electrons distribution of metal NPs under irradiation with different wavelengths (400 and 530 nm) and schemes that show how the hot electrons contribute to activate nitrobenzene and 4-nitrobenzyl alcohol reactant molecules. The hot electrons with energy above the energy level of the LUMO of the molecules adsorbed on the alloy NP can transfer into those orbitals, thereby potentially induce reaction. The calculated HOMO and LUMO for nitrobenzene and 4-nitrobenzyl alcohol are shown in Figure S6, SI. The LUMO of 4-nitrobenzyl alcohol molecule (LUMO 2) is higher than that of nitrobenzene molecule (LUMO 1), resulting two thresholds (threshold 1 and 2) for activation of the molecule, thus LUMO 2 requires light-excited energetic electrons to higher energy levels to activate the molecule. Considering the strongly chemisorbed adsorbates involves resonant electronic transitions between hybridized metal and adsorbate states, all the relative positions of the LUMO 1 for nitrobenzene and LUMO 2 for 4-nitrobenzyl alcohol from the Fermi level are only qualitative, and schematically show the relative positions of LUMO of the chemisorbed adsorbates.

When the hot electrons transfer into the lowest unoccupied molecular orbital (LUMO) of the reactant molecules adsorbed on the metal NPs,[35,37,39,42-44] which is associated with the N-O bonds, the bonds are weakened and the reduction is activated. Only the hot electrons with energy above a threshold that depends on the energy level of the LUMO level can inject into the adsorbed reactant LUMO to induce the reaction (see Figure 8d).[40] The calculated LUMO of 4-nitrobenzyl alcohol is higher (-2.7 eV) on the energy scale than that of nitrobenzene (-2.9 eV), thus the Fermi level of Au which is -5.1 eV, lies about 2.4 eV and 2.2 eV below the LUMO levels of 4-nitrobenzyl alcohol and nitrobenzene, respectively (Figure S6, SI). Only the hot electrons with energy at least 2.4 eV above the Au Fermi level can induce the reaction of 4-nitrobenzyl

alcohol. The Fermi level of the alloy NPs is slightly higher than that of Au, and thus, the energy required for the injection is reduced, < 2.4 eV. Shorter wavelengths more effectively generate hot electrons with the sufficient energy for the transfer (Figure 8d, left). The light absorption due to LSPR effect is intense and can excite a large number of metal electrons, but only to energy levels about 2 eV above the Fermi level (Figure 8d, right). Hence, the LSPR absorption is not as effective as the absorption of shorter wavelengths in driving the reduction of 4-nitrobenzyl alcohol, while it effectively drives the reduction of nitrobenzene, because nitrobenzene possesses a lower LUMO energy level. We have to bear in mind that the above discussion on the energetics of the reaction systems are semi-quantitative since the influence of the reactant

adsorption is not included. Another possible mechanism such as direct charge-transfer (direct excitation of electron to LUMO, without the formation of an excited electron distribution in the metal) may also be involved in the reaction.[45] The present study has limited capacity to distinguish between indirect and direct charge-transfer mechanism for the reactions. Nonetheless, the discussion reveals that the reduction reaction is mainly driven by hot electron transfer from alloy NP to the LUMO associated with the N-O bonds.

It is noted that high AQY values were found in the short wavelength range of the action spectra, in this range (400~450 nm), photons absorption may occur predominantly through interband transitions in AuCu NPs at the expense of LSPR excitation. The higher AQY values suggest that a more effective, adsorbate-specific, channel of transferring short wavelength photon energy into the activation of the N-O bonds on the NP surface. It is reported that metal NP size has effects on the wavelength-dependent photocatalytic reactions.[46] The small NPs (approximately 5.0 nm) have large fractions of surface atoms, making photon absorption likely to occur at surface atoms that are directly bonded to adsorbates, which may facilitate the direct photoexcitation of metal−adsorbate bonds to enhance the photocatalytic reaction on NP surface under irradiation.[46]

To further investigate the hot electron transfer process on the Au-Cu alloy NP surface, we simulated the molecular orbitals involved in hot electron transfer processes for nitrobenzene and 4-nitrobenzyl alcohol reactant molecules adsorbed on the Au-Cu cluster surface, respectively (see Figure S7, SI). The details of time-dependent density functional theory (TD-DFT) results are listed in Table S3-6, SI. The change in charge density distribution indicates electron transfer from the metal NP to the LUMO of the adsorbed reactant molecules under irradiation. These simulation results provide insight into the catalytic activity dependence on the intensity and wavelength of the incident light.

■ CONCLUSIONS

The study demonstrates that the Au-Cu alloy NPs on ZrO_2 is an excellent photocatalyst for the selective reduction of nitroaromatics to corresponding functionalized anilines as the sole product, driven by visible light irradiation, without requiring intensive heating and pressurized reagents. The reasons for the high efficiency of the photocatalytic reduction under these comparatively benign conditions were analyzed. During the photocatalytic reductions using this catalyst, the nitro group transformed directly to an amino group, rather than step-wise via a series of intermediates as described by Haber. The interaction between the nitro group and copper atoms is stronger than that between the nitro group and gold atoms, immobilizing the reactant. This effect facilitates direct reduction of the nitro group to an amino group and impedes the coupling reaction between two intermediate molecules. The reaction pathway change and mild reaction conditions

are the essential reasons for the high chemoselectivity towards anilines. The catalytic reaction rate can be further optimized by slight increase of the reaction temperature, while the high chemoselectivity to reduce the nitro groups is maintained. This study reveals that product chemoselectivity may be engineered simply by tailoring the bimetallic alloy NPs of the photocatalysts. This approach represents a new promising direction in the area of photocatalytic chemical transformations.[45] The knowledge acquired in this study could be useful to the development of new heterogeneous photocatalysts for the production of important chemicals, functionalized anilines and others, and to understand photocatalytic systems for organic reactions.

■ EXPERIMENTAL SECTION

Chemicals. Zirconium (IV) oxide (ZrO_2, <100 nm particle size, TEM), gold(III) chloride hydrate ($HAuCl_4 \cdot xH_2O$, 99.999% trace metals basis), Sodium borohydride ($NaBH_4$, ≥98.0%), copper(II) nitrate hydrate ($Cu(NO_3)_2 \cdot xH_2O$, ≥99.9% trace metals basis). All the chemicals used in the experiments were purchased from Sigma-Aldrich (unless otherwise noted) and used as received without further purification. The water used in all experiments was prepared by passing through an ultra-purification system.

Preparation of catalysts. Typically, $Au_{2.6}Cu_{0.4}@ZrO_2$ catalyst: ZrO_2 powder (1.0 g) was dispersed into a mixture of $HAuCl_4$ (13.2 mL, 0.01 M) and $Cu(NO_3)_2$ (6.25 mL, 0.01 M) aqueous solution under magnetic stirring at room temperature. A lysine (3 mL, 0.1 M) aqueous solution was then added into the mixture with vigorous stirring for 30 min, the pH value was 8−9. To this suspension, a freshly prepared $NaBH_4$ (2 mL, 0.35 M) aqueous solution was added drop wise. The mixture was aged for 24 h and then the solid was separated by centrifugation, washed with water (three times) and ethanol (once), and dried at 60 °C in a vacuum oven for 24 h. The dried powder was subjected to thermal treatment in a mixture of H_2 (5 vol%) and Ar at 450 °C for 0.5 h. The obtained powder was used directly as $Au_{2.6}Cu_{0.4}@ZrO_2$ catalyst. All the other catalysts were prepared via the same methods with different quantities of $HAuCl_4$ and $Cu(NO_3)_2$ aqueous solutions.

Characterization of catalysts. The size, morphology and composition of the catalyst samples was characterized with a JEOL2100 transmission electron microscopy (TEM), equipped with a Gatan Orius SC1000 CCD camera and an Oxford X-Max energy dispersive X-ray spectrometer (EDS). The Au and Cu contents of the prepared catalysts were determined by energy dispersion X−ray spectrum (EDS) technology using the attachment to a FEI Quanta 200 environmental scanning electron microscopy (SEM). Diffuse reflectance UV−visible (DR−UV−vis) spectra of the sample powders were examined with a Varian Cary 5000 spectrometer with $BaSO_4$ as a reference. The light absorption data was normalized with OriginPro 8 software, using the normalize methods: Normalize to [0, 1]. The normalized data was

plotted against wavelength to get the light absorption spectrum of the catalyst. X-ray photoelectron spectroscopy (XPS) data was acquired using a Kratos Axis ULTRA X-ray Photoelectron Spectrometer incorporating a 165 mm hemispherical electron energy analyzer. The incident radiation was Monochromatic Al Kα X-rays (1486.6 eV) at 225 W (15 kV, 15 ma). Narrow high-resolution scans were run with 0.05 eV steps and 250 ms dwell time. Base pressure in the analysis chamber was 1.0×10^{-9} torr and during sample analysis 1.0×10^{-8} torr. Peak fitting of the high-resolution data was carried out using the CasaXPS software.

Photocatalytic reactions. A 20 mL Pyrex glass tube was used as the reaction container, and after the reactants and catalyst had been added, the tube was sealed with a rubber septum cap. The reaction mixture was stirred magnetically and irradiated using a halogen lamp (from Nelson, wavelength in the range 400–800 nm, see Figure S8, SI) as the visible light source and the light intensity was measured to be 0.5 W/cm^2. The temperature of the reaction system was carefully controlled with an air conditioner attached to the reaction chamber. The control reaction system in the dark was maintained at the same temperature to ensure that the comparison is meaningful. All the reactions in the dark were conducted using a water bath placed above a magnetic stirrer to control the reaction temperature; the reaction tube was wrapped with aluminum foil to avoid exposure of the reaction mixture to light. At given irradiation time intervals, 0.5 mL aliquots were collected, and then filtered through a Millipore filter (pore size 0.45 μm) to remove the catalyst particulates. The liquid−phase products were analyzed by an Agilent 7820A gas chromatography (GC) with HP−5 column to measure the change in the concentrations of reactants and products. An Agilent HP5977A mass spectrometer attached to Agilent 7890B GC with HP−5MS column was used to identify the product. The acetone concentration was tested by Agilent 6890 GC with DB−Wax column.

Typical reaction conditions: nitrobenzene in isopropyl alcohol (IPA) solution (0.05 M) 2 mL (containing nitrobenzene 0.1 mmol), KOH in IPA solution (0.1 M) 0.25 mL (KOH 0.025 mmol), and catalyst 50 mg were added to the reaction tube, the temperature was 40 °C, under a 1 atm argon atmosphere, with a reaction time of 6 h. The reactions with other substrates were conducted under similar methods with some conditions changed slightly as noted in the reaction table.

Light emitting diode (LED) lamps (Tongyifang, Shenzhen, China) with wavelengths 400±5 nm, 470±5 nm, 530±5 nm, 590±5 nm, and 620±5 nm were used as the light source to investigate the catalytic performance under different wavelength (Action spectrum experiments). The light intensity of the LED light sources used for the wavelength dependent experiments was 0.2 W/cm^2, and the light intensity was maintained constant for each wavelength dependent experiment. The other reaction conditions were kept identical with the halogen lamp photocatalytic reactions. The AQY was calculated as: AQY = [($Y_{light} - Y_{dark}$) / (the number

of incident photons)] × 100%, where Y_{light} and Y_{dark} are the number of products formed under light irradiation and dark conditions, respectively. The number of products formed Y was calculated based on the following equation: Y = y × the mole of reactant × Avogadro constant, where the y is the product aniline yield for the reaction.

ASSOCIATED CONTENT

Supporting Information. Figures S1-8, Tables S1-7 and detailed DFT simulation parameters. This material is available free of charge via the Internet at http://pubs.acs.org.

AUTHOR INFORMATION

Corresponding Author

*E-mail: hy.zhu@qut.edu.au

Notes
The authors declare no competing finical interest.

ACKNOWLEDGMENT

REFERENCES

(1) Blaser, H. U.; Siegrist, U.; Steiner, H.; Studer, M. In *Fine Chemicals Through Heterogeneous Catalysis*, Sheldon, R. A., van Bekkum, H. Eds.; Wiley-VCH: Weinheim, Germany, 2001; p 389–406.

(2) Rosenblatt, D. H.; Burrows, E. P. *The Chemistry of Amino Nitroso and Nitro Compounds and their Derivatives*, Wiley-VCH: Chichester, 1982; p 1085.

(3) Corma, A.; Serna, P. *Science* **2006**, *313*, 332−334.

(4) Grirrane, A.; Corma, A.; Garcia, H. *Science* **2008**, *322*, 1661–1664.

(5) Jagadeesh, R. V.; Surkus, A. E.; Junge, H.; Pohl, M. M.; Radnik, J.; Rabeah, J.; Huan, H. M.; Schunemann, V.; Bruckner, A.; Beller, M. *Science* **2013**, *342*, 1073-1076.

(6) Westerhaus, F. A.; Jagadeesh, R. V.; Wienhöfer, G.; Pohl, M.-M.; Radnik, J.; Surkus, A.-E.; Rabeah, J.; Junge, K.; Junge, H.; Nielsen, M.; Brückner, A.; Beller, M. *Nat. Chem.* **2013**, *5*, 537− 543.

(7) Haber, F. *Z. Elektrochem.* **1898**, *22*, 506.

(8) Makosch, M.; Sa, J.; Kartusch, C.; Richner, G.; van Bokhoven J. A.; Hungerbuhler, K. *ChemCatChem.* **2012**, *4*, 59–63.

(9) Liu, X.; Li, H. Q.; Ye, S.; Liu, Y. M.; He, H. Y; Cao, Y. *Angew. Chem., Int. Ed.* **2014**, *53*, 7624–7628.

(10) Blaser, H. U. *Science* **2006**, *313*, 312–313.

(11) Corma, A.; Concepción, P.; Serna, P. *Angew. Chem., Int. Ed.* **2007**, *46*, 7266-7269.

(12) Zhu, H. Y.; Ke, X. B.; Yang, X. Z.; Sarina, S.; Liu, H. W. *Angew. Chem., Int. Ed.* **2010**, *49*, 9657–9661.

(13) Chen, X.; Zhu, H. Y.; Zhao, J. C.; Zheng, Z. F.; Gao, X. P. *Angew. Chem., Int. Ed.* **2008**, *47*, 5353–5356.

(14) Sarina, S.; Waclawik, E. R.; Zhu, H. Y. *Green Chem.* **2013**, *15*, 1814–1833.

(15) Wang, C.; Astruc, D. *Chem. Soc. Rev.* **2014**, *43*, 7188–7216.

(16) Khanal, S.; Bhattarai, N.; McMaster, D.; Bahena, D.; Velazquez-Salazar, J. J.; Jose-Yacaman, M. *Phys. Chem. Chem. Phys.* **2014**, *16*, 16278–16283.

(17) Liu, X.; Wang, A.; Li, L.; Zhang, T.; Mou, C. Y.; Lee, J. F. *J. Catal.* **2011**, *278*, 288–296.

(18) Xu, Z.; Lai, E.; Shao-Horn Y.; Hamad-Schifferli, K. *Chem. Commun.* **2012**, *48*, 5626–5628.

(19) Wang, L.; Yang, J. C. *J. Mater. Res.* **2005**, *20*, 1902–1909.

(20) Guo, X. N.; Hao, C. H.; Jin, G. Q.; Zhu, H. Y. Guo, X. Y. *Angew. Chem., Int. Ed.* **2014**, *53*, 1973–1977.

(21) Gonçalves, R. V.; Wojcieszak, R.; Wender, H.; Sato B. Dias, C.; Vono, L. L. R.; Eberhardt, D.; Teixeira, S. R.; Rossi, L. M. *ACS Appl. Mater. Interfaces* **2015**, *7*, 7987–7994.

(22) Schünemann, S.; Dodekatos, G.; Tüysüz, H. *Chem. Mater.* **2015**, *27*, 7743–7750.

(23) Sugano, Y.; Shiraishi, Y.; Tsukamoto, D.; Ichikawa, S.; Tanaka, S.; Hirai, T. *Angew. Chem., Int. Ed.* **2013**, *52*, 5295–5299.

(24) Marimuthu, A.; Zhang, J.; Linic, S. *Science*, **2013**, *339*, 1590–1593.

(25) Cano, I.; Huertos, M. A.; Chapman, A. M.; Buntkowsky, G.; Gutmann, T.; Groszewicz, P. B.; van Leeuwen, P. W. N. M. *J. Am. Chem. Soc.* **2015**, *137*, 7718–7727.

(26) Pramanik, S.; Mishra, M. K.; De, G. *CrystEngComm.* **2014**, *16*, 56-63.

(27) Lide, D. R. *Section 9, Molecular Structure and Spectroscopy; Electronegativity*, CRC Handbook of Chemistry and Physics, 84th Edition. CRC Press: Boca Raton, Florida, 2003; p 9-74.

(28) Abad, A.; Concepción, P.; Corma, A.; García, H. *Angew. Chem., Int. Ed.* **2005**, *44*, 4066–4069.

(29) Ellis, F. *Paracetamol: a Curriculum Resource*, Royal Society of Chemistry: Cambridge, 2002; p 3–12.

(30) Saha, A.; Adamcik, J.; Bolisetty, S.; Handschin, S.; Mezzenga, R. *Angew. Chem., Int. Ed.* **2015**, *54*, 5408–5412.

(31) Li, A.; Luo, Q.; Park, S. -J.; Cooks, R. G. *Angew. Chem., Int. Ed.* **2014**, *53*, 3147–3150.

(32) Wang, X.; Liu, D.; Song, S.; Zhang, H. *J. Am. Chem. Soc.* **2013**, *135*, 15864–15872.

(33) Linic, S.; Christopher, P.; Ingram, D. B. *Nat. Mater.* **2011**, *10*, 911–921.

(34) Christopher, P.; Xin, H. L.; Marimuthu, A.; Linic, S. *Nat. Mater.* **2012**, *11*, 1044–1050.

(35) Xiao, Q.; Jaatinen, E.; Zhu, H. Y. *Chem.–Asian J.* **2014**, *9*, 3046–3064.

(36) Xiao, Q.; Liu, Z.; Bo, A.; Zavahir, S.; Sarina, S.; Bottle, S.; Riches, J. D.; Zhu, H. Y. *J. Am. Chem. Soc.* **2015**, *137*, 1956–1966.

(37) Sarina, S.; Zhu, H. Y.; Xiao, Q.; Jaatinen, E.; Jia, J.; Huang, Y.; Zheng, Z.; Wu, H. *Angew. Chem., Int. Ed.* **2014**, *53*, 2935–2940.

(38) Sarina, S.; Zhu, H.; Jaatinen, E.; Xiao, Q.; Liu, H.; Jia, J.; Chen, C.; Zhao, J. *J. Am. Chem. Soc.* **2013**, *135*, 5793–5801.

(39) Long, R.; Li, Y.; Song, L.; Xiong, Y. *Small* **2015**, *11*, 3873–3889.

(40) Brus, L. *Acc. Chem. Res.* **2008**, *41*, 1742–1749.

(41) Smith, J. G.; Faucheaux, J. A.; Jain, P. K. *Nano Today* **2015**, *10*, 67–80.

(42) Kale, M. J.; Avanesian, T.; Christopher, P. *ACS Catal.* **2014**, *4*, 116–128.

(43) Zhao, L. B.; Huang, Y. F.; Liu, X. M.; Anema, J. R.; Wu, D. Y.; Ren, B.; Tian, Z. Q. *Phys. Chem. Chem. Phys.* **2012**, *14*, 12919–12929.

(44) Zhao, L. B.; Zhang, M.; Huang, Y. F.; Williams, C. T.; Wu, D. Y.; Ren, B.; Tian, Z. Q. *J. Phys. Chem. Lett.* **2014**, *5*, 1259–1266.

(45) Linic, S.; Aslam, U.; Boerigter, C.; Morabito, M. *Nat. Mater.* **2015**, *14*, 567–576.

(46) Kale, M. J.; Avanesian, T.; Xin, H.; Yan, J.; Christopher, P. *Nano Lett.* **2014**, *14*, 5405–5412.

Table of Contents (TOC) graphic